Atomic Size and Local Order Effects on the High Temperature Strength of Binary Mg Alloys

Saeideh Abaspour, Victor Zambelli, Matthew Dargusch, Carlos H. Cáceres

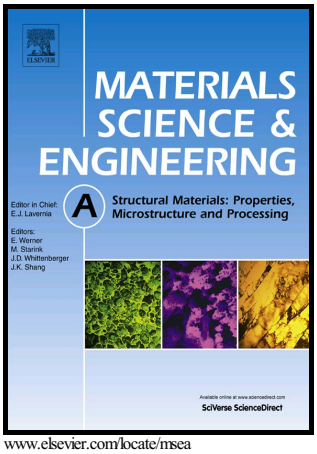

www.elsevier.com/locate/msea

PII: S0921-5093(16)30771-7
DOI: http://dx.doi.org/10.1016/j.msea.2016.07.019
Reference: MSA33850

To appear in: *Materials Science & Engineering A*

Received date: 25 November 2015
Revised date: 4 July 2016
Accepted date: 6 July 2016

Cite this article as: Saeideh Abaspour, Victor Zambelli, Matthew Dargusch and Carlos H. Cáceres, Atomic Size and Local Order Effects on the High Temperature Strength of Binary Mg Alloys, *Materials Science & Engineering A* http://dx.doi.org/10.1016/j.msea.2016.07.019

Atomic Size and Local Order Effects on the High Temperature Strength of Binary Mg Alloys

Saeideh Abaspour,[a,b,*] Victor Zambelli,[a] Matthew Dargusch,[b] Carlos H. Cáceres[a]

[a]ARC-Centre of Excellence for Design in Light Metals, Materials Engineering, School of Engineering, The University of Queensland, Brisbane, QLD 4072, Australia

[b]Queensland Centre for Advanced Materials Processing and Manufacturing (AMPAM), The University of Queensland, Australia

Abstract:

The solid solution strengthening introduced by Ca (0.6 and 0.9 at.%) and Sn (0.5 to 2.5 at.%) was studied through tensile, compression and stress relaxation tests at room temperature, 373K (100°C) and 453K (180°C) on solution heat-treated and quenched specimens and compared with existing data for binary alloys containing Ca, Sn, Y, Gd, Nd, Zn and Al as well as for AZ91 alloy. At room temperature the solution-hardening rate introduced by Ca and Sn was much higher than that of Al, matching those of Y, Gd and Zn. Calcium also reduced the tension/compression asymmetry. At high temperature Ca effectively prevented stress relaxation, nearly matching Y, Gd and Nd. Tin was less effective, but still outperformed Al and AZ91 at low stresses. The effects at room and high temperature introduced by Ca and Sn appeared consistent with the presence of short-range order, in line with those introduced by Y, Nd, Gd and Zn. The larger than Mg atom size of Ca, Nd, Gd and Y can be expected to intensify the local order by strengthening the atomic bonds through its effects on the local electron density, accounting for their greater strengthening at high temperature. For given difference in atomic size, the effects on the local order are expected to be lesser for smaller sized atoms like Sn and Zn, hence their more subdued effects.

Keywords: Mg-Ca alloys; Creep strength; Short Range Order (SRO); Mg-RE alloys; Stress relaxation, Solid solution hardening.

*Corresponding author, e-mail: s.abaspour78@gmail.com

Introduction

The design of creep resistant Mg alloys often aims at strengthening the α-Mg matrix by solid solution by, e.g., Al, and/or precipitation hardening via selected trace solute additions [1, 2]. In the Mg-Al system, examples of trace additions are Ca [3], Sr [4], RE [5], Si [6, 7], Sb [8, 9], Sn [10, 11].

Calcium makes a most attractive option since it provides acceptable levels of castability, and increased corrosion and creep resistance at low cost [12] in comparison with the RE. Recent developments involving additions of Ca to Mg-Al resulted in the high pressure die casting MRI230D and AXJ350 alloys [13, 14] (1.2 at.% in MRI230D and 2 at.% in AXJ530), both significantly more creep resistant than AE42 alloy, usually considered a standard [14-16]. The role played by Ca in increasing the creep strength, however, remains unclear. It has been claimed that Ca introduces a strong solid solution hardening [14], whereas the dislocation pinning by $(Mg,Al)_2Ca$ precipitates was credited for the decreased creep rate [13]. Alternatively, the increased creep resistance has been ascribed to the lower diffusion rate caused by the larger atomic size of Ca in comparison with Mg [2, 17, 18].

No data are available for the strengthening introduced by Ca in solution in cast (i.e., texture-free) binary alloys, although data obtained from extruded Mg-Ca alloys suggests that the solid solution hardening rate is comparable to those of Y, Gd and Zn, and well above that of Al in solution, see ref. [19] for a detailed discussion. Against the claim of reduced diffusivity, it has been recently pointed out, based on published data on HCP-Zr, that the mobility of substitutional solutes is not necessarily related to the atomic size [19, 20].

The presence of Ca in solution in wrought alloys has also the rather peculiar effect of weakening the usual basal texture, similarly to what is observed in Mg-RE alloys [18, 21]. The texture weakening effect of Ca has also been ascribed to atom size driven segregation [21-23]. However, solute segregation in the form of dynamic strain aging (serrated flow) in AZ91 [24-26], and in several other alloys [1, 27-30] is also normally reported but without any texture weakening effects, questioning the fundamental assumption of this claim. On a closer look, such degree of commonality of effects, i.e., strong solid solution hardening and texture weakening effects, points out to a deeper similarity between Ca and the RE, which are also known to increase the creep resistance even when present in very limited concentration [2, 19, 31, 32].

Mg-Sn alloys have also received considerable attention concerning room and high temperature (HT) applications [1, 2, 10, 11, 33, 34]. At room temperature (RT), recent experiments [35] on binary solid solutions suggested that Sn introduces a rather weak solid solution hardening in comparison with Zn, although those experiments were marred by a very large grain size that questioned whether the data were valid for polycrystals [19].

In more recent work involving dilute binary alloys [19, 31] it has been argued that short range order (SRO) is a dominant reason for the increased strength in comparison with Mg-Al (which represents random solid solution hardening [36]) at both RT and HT, of a wide range of multicomponent alloys containing Y, Gd, Nd, Zn, Ca and Sn. The presence of SRO has been confirmed by diffuse x-ray scattering in binary solid solutions of Mg and Gd [37], Er [37], Sn [38, 39], Tb [40], In [41] and Bi [42]. SRO has been observed as well in liquid Mg-Zn [43] and in aged Mg-5at.%Gd [44].

The tendency to develop SRO in Mg alloys has been justified from first principles by atomic level thermodynamics through the Miedema phenomenological scheme [19], illustrated by Fig. 1 and briefly described below.

The scheme introduced in the 1970's by Miedema et al. involves two parameters [45-52]: the work function, ϕ^*, (closely related to Pauling's electronegativity value), and the electron density at the boundary of the Wigner–Seitz (W-S) atomic cell, $\Delta n_{WS}^{1/3}$. The sign and magnitude of the enthalpy of formation, ΔH, of a metallic solution can be obtained based on these two parameters alone, anticipating the relative tendency to form either ordered ($\Delta H < 0$), random ($\Delta H = 0$) or immiscible solutions ($\Delta H > 0$). For any given binary alloy, in both the solid and liquid state, when forming an equi-atomic compound, ΔH is given by [46-48, 53-56]:

$$\Delta H = -P(\Delta\varphi^*)^2 + Q(\Delta n_{WS}^{1/3})^2 - R\,, \qquad (1)$$

where P and Q are constants related to each other as Q/P = 9.4 $(eV)^2(d.u.)^{2/3}$. Q/P is the slope of the straight line separating positive and negative ΔH-values (i.e., the line itself is the locus of alloys with $\Delta H = 0$, for which complete miscibility can be expected). The parameter R, called the hybridization term, enters the equation only when transition metals are alloyed with non-transition metals. R is small for Mg and has been neglected [46] for Fig. 1. The diagram of Fig. 1 sorts out the potential solutes according to whether they sit on the positive, or North/South, or the negative, or East/West sectors, where the positive/negative sign applies to the ΔH- values of the particular solute/host combination.

In Fig. 1 the solutes studied in the present work (Ca and Sn) are sorted out together with selected ones from prior work [19, 31] for reference. The solutes that belong to the South sector, i.e., the RE, Y and Ca, are more electropositive and larger than Mg, whereas the ones on the North are less so, but all of them mix with a negative ΔH-value, hence all of them have a tendency to develop order in solution solutions. The phase diagram for solutes on the North or South sectors typically exhibits a high melting point intermetallic bounded by deep eutectics. Thorium and Mn exemplify solutes with a positive ΔH-value, sitting on the West sector in this case, and are characterised by a tendency to phase separation and a single eutectic phase diagram.

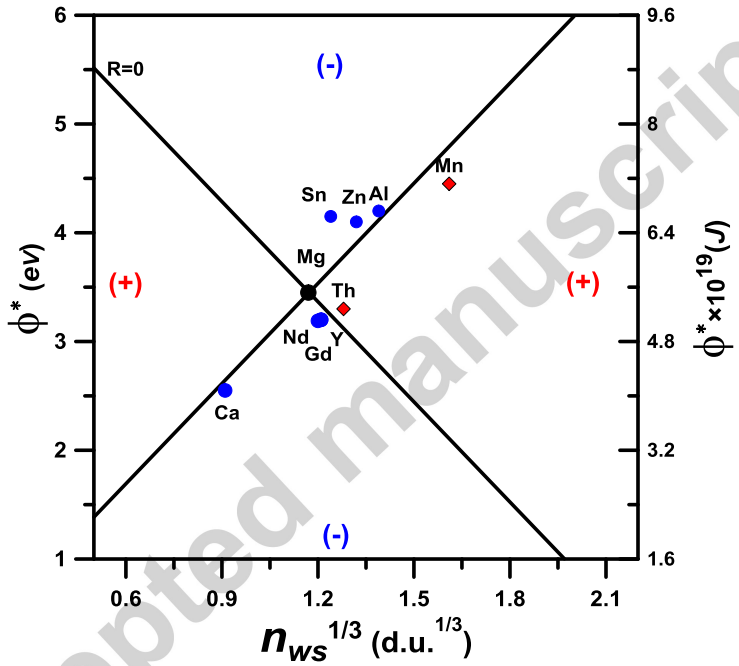

Figure 1. The Miedema scheme for Mg as a host, for selected solutes, created assuming R=0 in Eq. 1. Coordinates for the data points from [48].

The experimental results of a parallel study [31] on stress relaxation of binary alloys at high temperatures is much reduced for Y, Gd and Nd, i.e., for solutes sitting on the South sector of the Miedema diagram, than for Sn and Zn, which belong in the North sector. This was in spite of the fact that solid solution hardening introduced at RT by any one of them was of comparable in strength and consistent with the presence of SRO, see, e.g., Fig. 3 in [19]. Differences between calculated and experimental values of the enthalpy of formation in liquid alloys are attributed to ordering effects in the solid versions of the alloys [57], but in this case this would not explain the systematically lower HT

strength (or increased stress relaxation) of the elements sitting on the North in comparison with those on the South. A possible explanation for this inconsistency was put forward by Zhang and Liu [58] involving atomic sizes: an increased solute size should shift the electron clouds in the W-S cells further apart, increasing the binding energy with the host. For given atomic size difference, the intensity of the SRO should therefore be greater for atoms sitting on the South sector, i.e., bigger than Mg, than those sitting on the North sector, i.e., smaller than Mg. In simpler terms, solutes sitting in the South sector should result in greater creep resistance.

Sn and Ca were selected for the present work in order to test the above hypotheses, i.e.: (i) the solid solution hardening rate introduced by both solutes should be consistent with SRO at RT, hence roughly equivalent, but, (ii) since Ca (1.97 pm) is larger than Mg (1.598 pm), whereas Sn is smaller (1.542 pm) (atomic radii data from [59]) the hardening due to SRO at HT introduced by the former should be greater.

Binary alloys with predetermined concentrations were cast and the solid solution hardening determined at room temperature and, through stress relaxation testing, at high temperatures (373K (100°C) and 453K (180°C)). The results were compared with existing data for alloys of both Sn and Ca as well as for Y, Gd, Nd, Zn and Al, with especial attention to the alleged effects of atomic size on the local order.

Experimental Procedure

Binary alloys with nominal compositions 0.5, 1.0, 1.5 and 2.5 at.% Sn and 0.6 and 0.9 at.% Ca were produced by melting commercially pure Mg, Sn and a Mg-Ca master alloy (1:4 Ca:Mg) in a steel crucible coated with boron nitride, using an electric furnace. SF_6+CO_2 was used as protective atmosphere. The liquid was poured at 1008-1023K (735-750°C) under an argon atmosphere into cylindrical steel moulds of 70 mm length and 45 mm diameter, preheated to 473K (200°C). The cast cylinders were solution heat-treated under an Ar atmosphere according to the times and temperatures listed in Table 1, and quenched into water. Samples for metallography were prepared following standard procedures and etched using an acetic–picric acid mixture (20 ml acetic acid, 3 g picric acid, 20 ml H_2O and 50 ml ethanol). The linear intercept method in accordance with ASTM E112-88 was used to determine the grain size, counting not fewer than 200 boundaries in each specimen. The grain size and compositions are also listed in Table 1. The lack of orientation texture on the cast grain microstructure was verified in a parallel study involving similarly produced Mg-Gd binary alloys [60].

Tensile testing at room temperature was carried out using cylindrical specimens, with a gauge length of 24 mm and 6 mm in diameter, on a screw-driven machine at 0.2 mm/min crosshead speed. A 12.5 mm knife-edge extensometer was attached to the gauge length. Compression testing at 298K (25°C), 373K (100°C) and 453K (180°C) was performed on cylindrical specimens 18 mm in height and 9 mm in diameter. No extensometer was used and the compressive strain was calculated based on the crosshead displacement. Stress relaxation was carried out in compression at 453K (180°C), after deforming at an applied crosshead speed of 0.2 mm/min (initial strain rate = 1.85×10^{-4} s^{-1}) up to a strain of 0.02 and the machine stopped for 1800 s (30 min).

Table 1. Solute concentration of the binary alloys studied, as determined by inductively coupled plasma atomic emission spectroscopy (ICP-AES); and the respective grain sizes and solution heat treatments (time and temperature) schedules.

Solute content (nominal, at.%)	Solute content (actual, at.%)	Grain size (μm)	Time (h)	Temperature K (°C)
2.5%Sn	2.5%Sn	127	12	773(500)
1.5%Sn	1.54%Sn	140	10	773 (500)
1.0%Sn	1.1%Sn	150	8	753 (450)
0.5%Sn	0.7%Sn	108	8	753 (450)
0.9%Ca	0.82%Ca	120	12	773(500)
0.6%Ca	0.56%Ca	130	8	773 (500)

Results

Figure 2 shows the grain microstructures of the alloys tested.

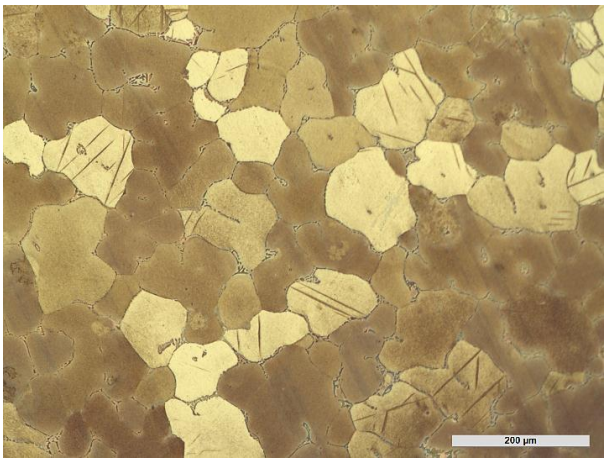

(a)

(b)

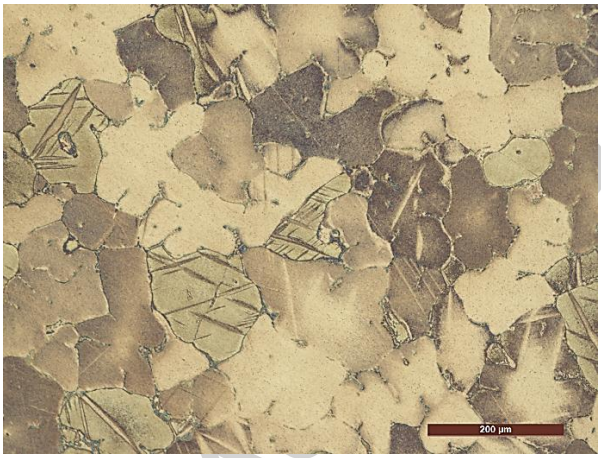

(c)

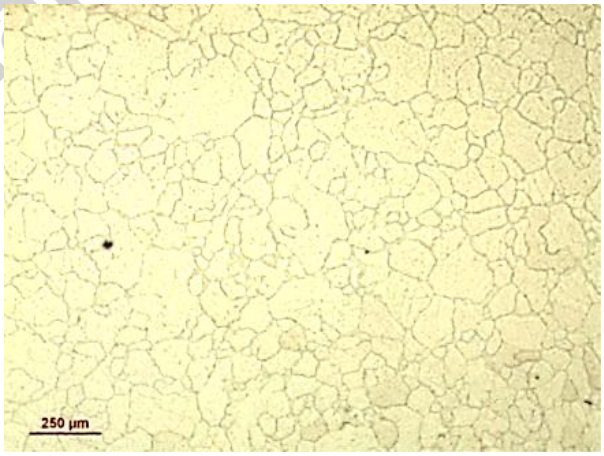

(d)

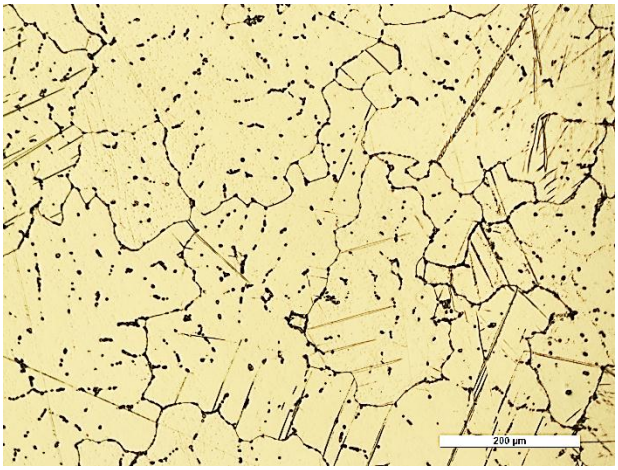

(e)

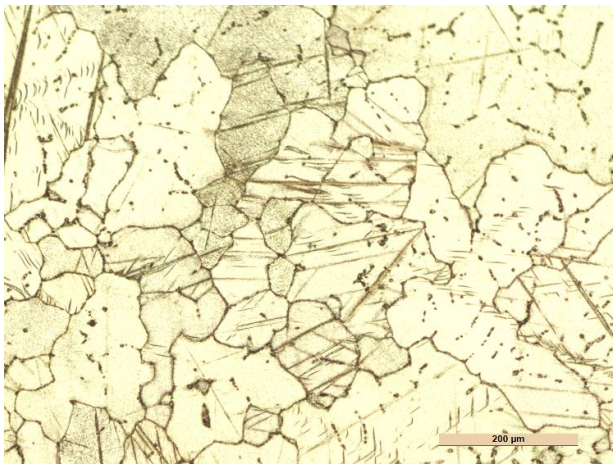

(f)

Figure 2. Optical photomicrographs of the alloys studied, in the solution heat-treated condition a) Mg-2.5Sn, b)Mg-1.5Sn, c)Mg-1Sn, d) Mg-0.7Sn, e)Mg-0.82Ca, f) Mg-0.56Ca.

The flow behaviour of the alloys of Table 1 is shown in Fig. 3. Flow curves for Mg-Y and AZ91 alloys are included for comparison in Figs. 3-b and 3-d. Fig. 3-c compares the compression behaviour of the most diluted and concentrated Mg-Sn alloys between 298-453K (25-180°C).

At RT (Figs. 3-a and 3-b) both Mg-Sn and Mg-Ca exhibited a linear hardening regime up to 0.1 strain in compression and up to about 0.06 strain in tension (in the latter the tensile ductility was the limiting factor). Increasing the temperature (Figs 3-c and 3d) shortened the length and lowered the slope of the linear regime.

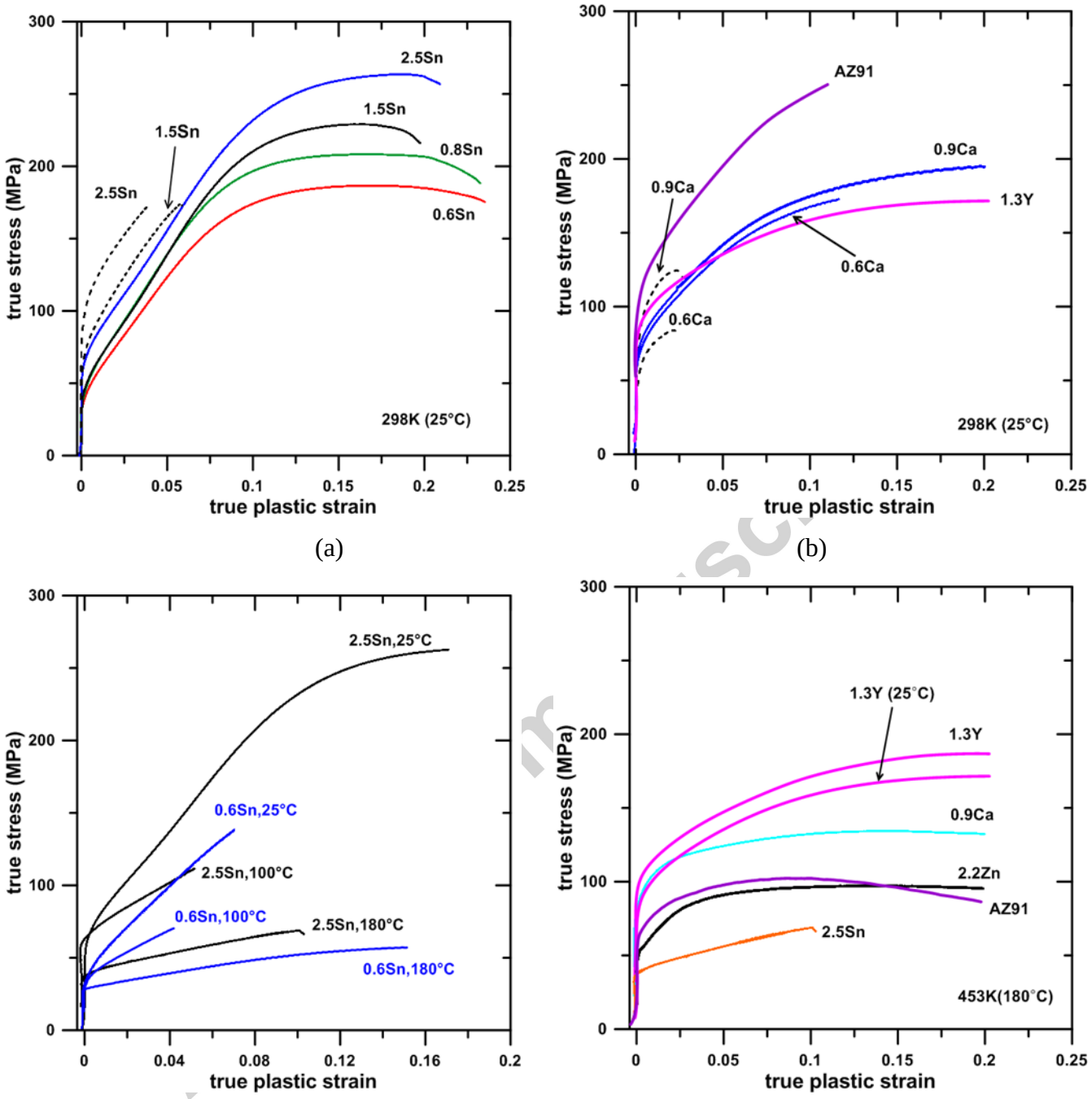

Figure 3. The flow behaviour at room and high temperature of the alloys studied. The dashed lines indicate tensile testing.

In Fig. 4-a the solid solution hardening at RT introduced by Sn (triangles) and Ca (circles) in the present experiments is compared with equivalent data from the literature. The solid and open diamonds

represent extruded and solution heat-treated Mg-Ca alloys, in tension and compression, respectively. [1] The much finer grain size and orientation texture of those specimens account for their higher average flow strength in comparison with the current (texture-free) experiments.[2] The crosses correspond to tensile yield strength of Mg-Sn specimens with extremely large grain size from ref. [26], hence the lower flow stress in comparison with the present values, as mentioned in the introduction. The comparison between tensile and compressive yield strength shows that while Ca virtually eliminates the t/c asymmetry, Sn has little or no effects upon it.

In Fig. 4-b the comparison is extended to existing tensile data for Y, Gd, Zn and alloy AZ91 (all obtained using cast alloys, solution heat-treated and quenched). Although Ca hardens Mg more than Sn, both sets of data points are within the range defined by Zn, Y and Gd, and all well above that of Al (or AZ91) which represents random solid solution [36].

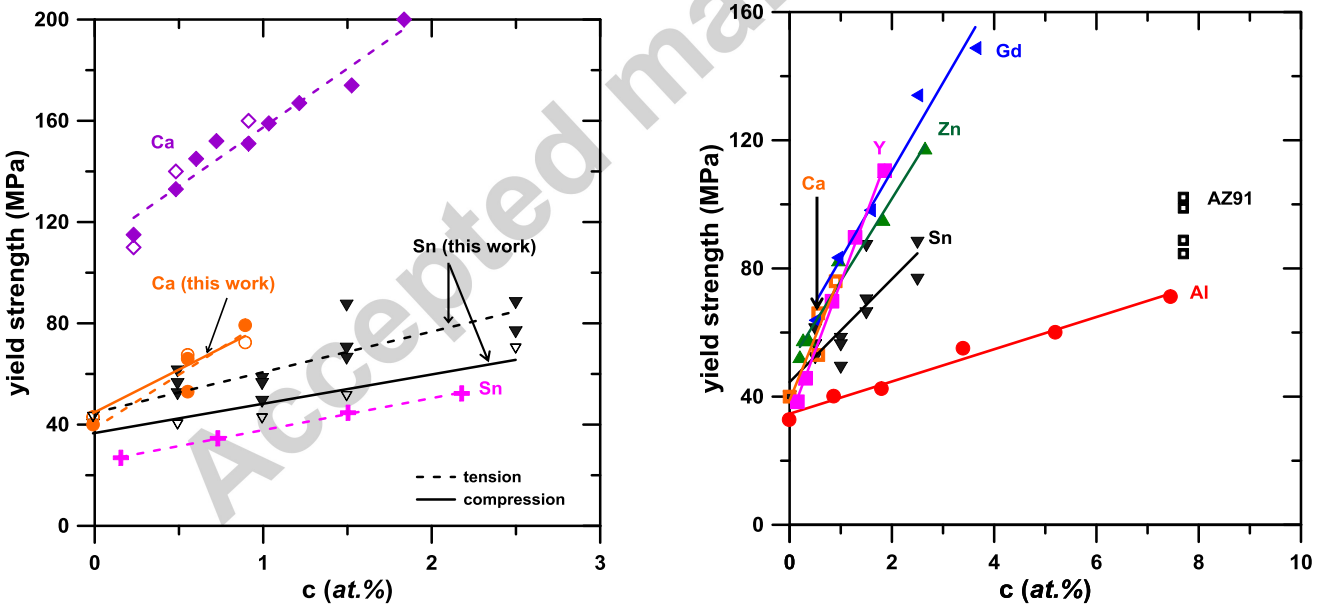

(a) (b)

Figure 4: (a) The strength in tension and compression of Mg-Sn and Mg-Ca solid solutions (circles and triangles) for the present experiments and data from: [35](Mg-Sn, crosses), [21](Mg-Ca, open

[1] *The open diamonds were mistakenly reported by the present authors as tensile data in Fig. 3 of ref. [19].*

[2] *The yield strength in the same experiments (open diamonds) was reported as independent of the Ca content in the original publication [21] but with little justification.*

diamonds), [61](solid diamonds). The data for pure Mg were taken from [62] (grain size 105 μm); (b) Comparison of the tensile data only with other cast binary alloys and alloy AZ91, sourced from:[62] (Mg-Zn and AZ91);[36] (Mg-Al);[63] (Mg-Gd); [29] (Mg-Y). The AZ91 alloy data points were plotted according to the alloy's nominal Al content (7.7at.%).

The stress relaxation behaviour, exemplified in Fig. 5 for an applied strain of 0.02, was closely consistent with the monotonic strength data of Fig. 4: the stress relaxation of Ca was comparable to that of Nd, Gd and Y. Sn relaxed faster than Ca, at a rate comparable with AZ91.

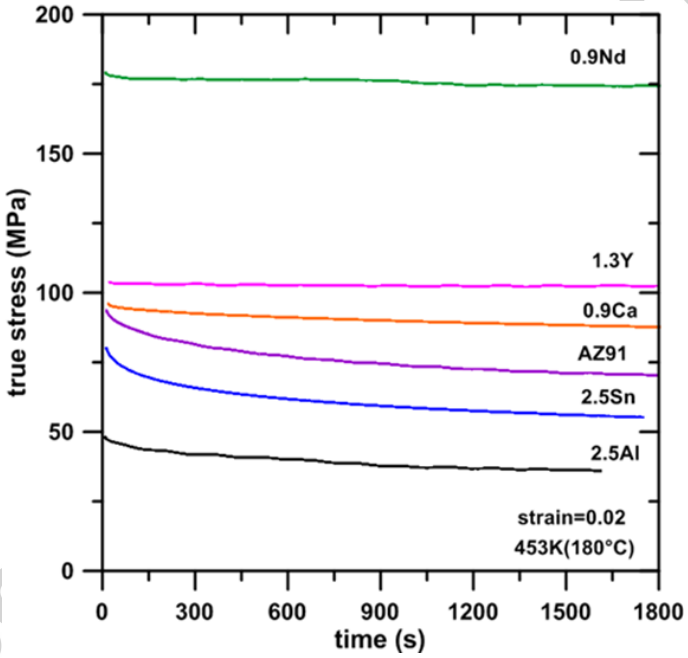

Figure 5. Stress relaxation curves at 453K (180°C) at an applied strain of 0.02. The figure preceding each solute is its concentration in at.%.

Figures 6-a through 6-c make evident the applied stress dependence of the strength-temperature relationship for each solute. Figure 6-a identifies an athermal regime at yield (applied strain = 0.005) extending beyond 453K (180°C) for all solutes save for Sn and especially less so for alloy AZ91. At higher applied strains, Figs. 6-b and 6-c, the athermal regime was preserved to 453K (180°C) only for Nd, Gd, Y and Ca, with the rest of the solutes exhibiting an increased loss of strength.

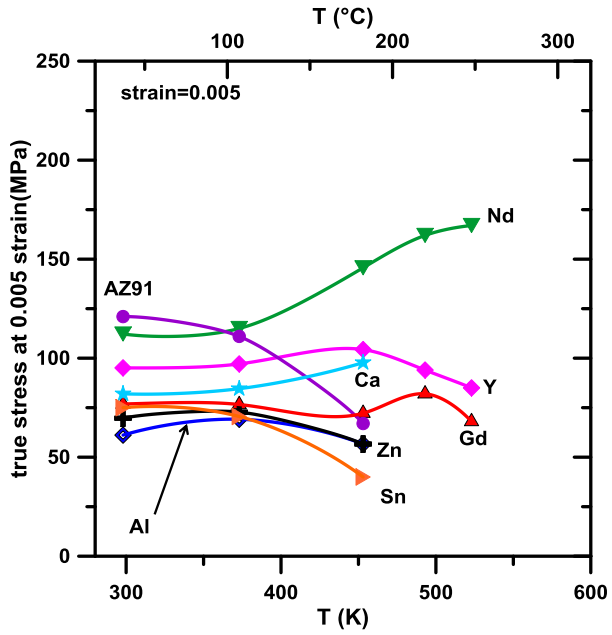

(a)

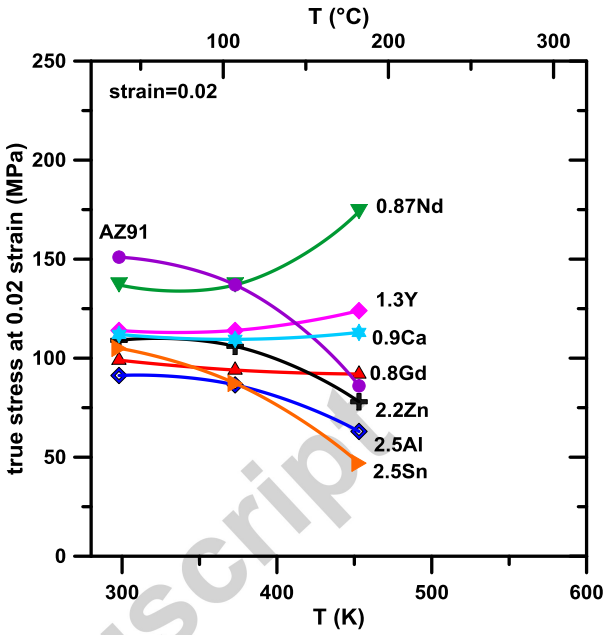

(b)

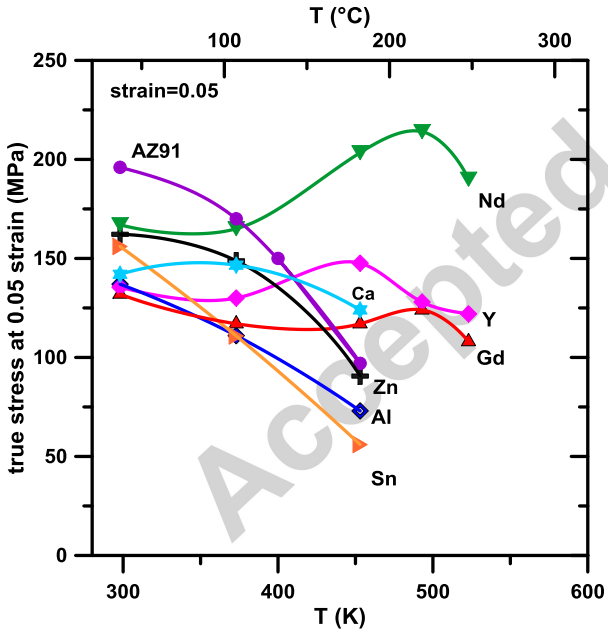

(c)

Figure 6. The flow stress of the alloys as a function of the temperature, for applied compressive strains of (a) 0.005; (b) 0.02; (c) 0.05.

Discussion

Room temperature strength

From Fig. 4-b the close similarity in the hardening introduced by Ca, Sn, the RE, Y and Zn is evident. This similarity can be accounted for from first principles [19, 31, 62] through SRO, as already argued in relation to the Miedema scheme and Fig. 1. The linear strain-hardening regime exhibited by the RT deformation curves at low strains in Fig. 3 is an indication of athermal forest hardening stemming from a stable forest dislocation substructure, a conclusion consistent with the presence of SRO [31, 32, 64-66]. Figures 3-c and 3-d show that some of the solutes, particularly Y, preserve the linear hardening regime up to 453k (180°C). Mg-Sn exhibits linear hardening at higher temperatures, but at a much reduced flow strength (Fig. 6-c), which accounts for the fast relaxation observed in Fig. 5 at a relatively high applied stress.

Figure 4-a, on the other hand, shows that the effects of Ca and Sn upon twinning, manifest through the t/c asymmetry, are widely different: while Ca virtually eliminates the t/c asymmetry, it remains unchanged for Sn. As stated in the introduction, the strong effect of Ca upon twinning, which ultimately reflects on the weakening of texture, brings it closer to the other solutes sitting on the South sector of the Miedema diagram, i.e. the RE and Y. Reasons for this similarity are discussed next in connection with the HT behaviour in general.

High temperature strength

In previous work [31], following [62], a number of binary alloys were ranked based on the strength of the respective SRO according to the expression

$$\tau_{SRO} \sim [\Delta H * c(1-c)]^2 \quad , \qquad (2)$$

where τ_{SRO} is the increase in the CRSS in the basal plane due to SRO, c is the solute concentration (see Table 1 in [31] for details concerning solutes other than Sn and Ca) and ΔH the enthalpy of solution calculated according to Eq. 1. The analysis indicated as the most effective solutes those combining a high ΔH-value with a relatively high solubility at the test temperature.

Neither Eq. (1) nor Eq. (2) allow for atomic size effects. As mentioned in the introduction, Zhang and Liu [58] suggested that atomic size should be incorporated into the formulation. They did so through a pre-factor to Eq. 1 that increases the enthalpy of formation in proportion to both the difference in size

and the actual size of the larger atom involved. These assumptions have a rather dramatic effect, illustrated by Fig. 7, where the standard and size corrected Miedema ΔH-values are plotted. The standard ΔH values show no preferential behaviour as functions of the atomic size, unlike the corrected ones that do so. In more practical terms, the smaller atoms, i.e., those sitting on the North sector, of the Miedema scheme exhibit a reduced (size corrected) ΔH-value whereas the bigger ones exhibit a relatively larger one.

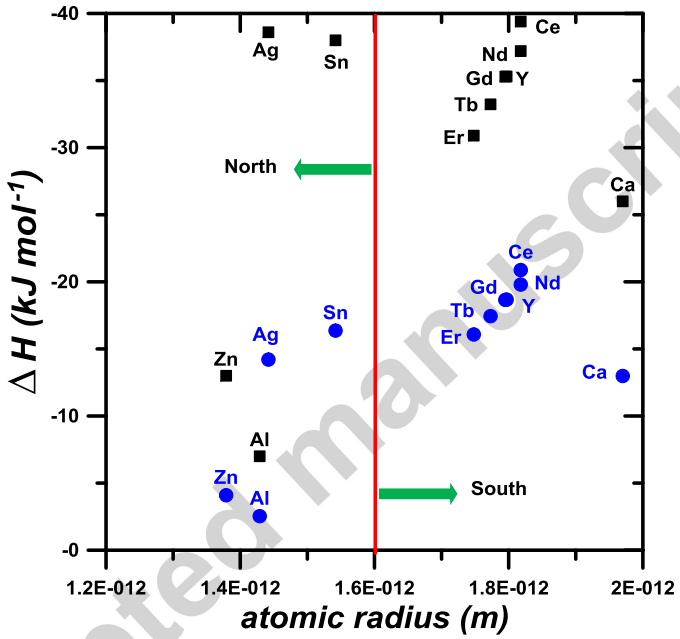

Figure 7. The enthalpy of formation of Mg alloys as a function of the size of the solute atoms. The standard Miedema ΔH-values (squares), sourced from [45]; the values corrected for atomic size effects (circles) were obtained according to the model by Zhang and Liu [58], see Appendix A for details. The vertical line identifies the locus of Mg and separates the North sector from the South sector in the Miedema scheme of Fig. 1.

The current results and equivalent data collected in the prior experiments of [31] are compared in Fig. 8 with the predictions of Eq. 2 obtained using the ΔH –values corrected for atom size effects (a similar figure created using the standard (uncorrected) Miedema ΔH-values in Eq. 2 can be seen in ref. [31]). In Fig. 8 the experimental data are plotted as the reciprocal of the stress drop, $(1/\Delta\sigma_{relaxation})$, during the

stress relaxation tests. The calculated (circles) and measured (diamonds) data generally match it other, strongly supporting the hypotheses behind Eq. 2, namely that SRO is a dominant strengthening mechanism when present. Figure 8 indicates that the best creep performance is to be expected for Y and Gd due to their strong SRO, whereas Ca should exhibit SRO at a level comparable to that of Nd. In general terms, all solutes should perform much better than Al, which represents a near random solid solution. Figure 8 also accounts for the fact that despite the high solid solubility of Al, hence its measurable strengthening effects at room temperature, the hardening does not extend to high temperatures. In practical terms, the high RT strength of AZ91 resulting from its extensive random solid solution hardening projects onto the high temperature behaviour only through a high yield strength, but necessarily with the poor creep performance of a random solid solution shown by Fig. 6-c, something repeatedly pointed out in the literature [67].

The overall behaviour of the alloys of Fig. 8 provides strong support for the hypothesis concerning atomic size effects on SRO: atoms larger than the host can be expected to develop a relatively stronger SRO, whereas smaller ones will develop a relatively weaker one. The greater effect of Ca upon the t/c asymmetry in Fig. 4-a is similarly consistent with a stronger effect through its size-enhanced SRO upon {10-20} twinning, matching the effects of Gd, Nd or Y, as discussed in detail in [60] .

The joint rationalisation through SRO (including the atomic size effects) of the increased creep strength and reduced t/c asymmetry introduced by Ca is made more significant by the fact that it dismisses unsupported claims in the literature aimed to account the effects through either a reduced diffusivity due to a larger atom size [2], the pinning of dislocations and grain boundaries by atomic size driven segregation [21-23] or unconfirmed valence mechanisms [68], as already discussed in [19].

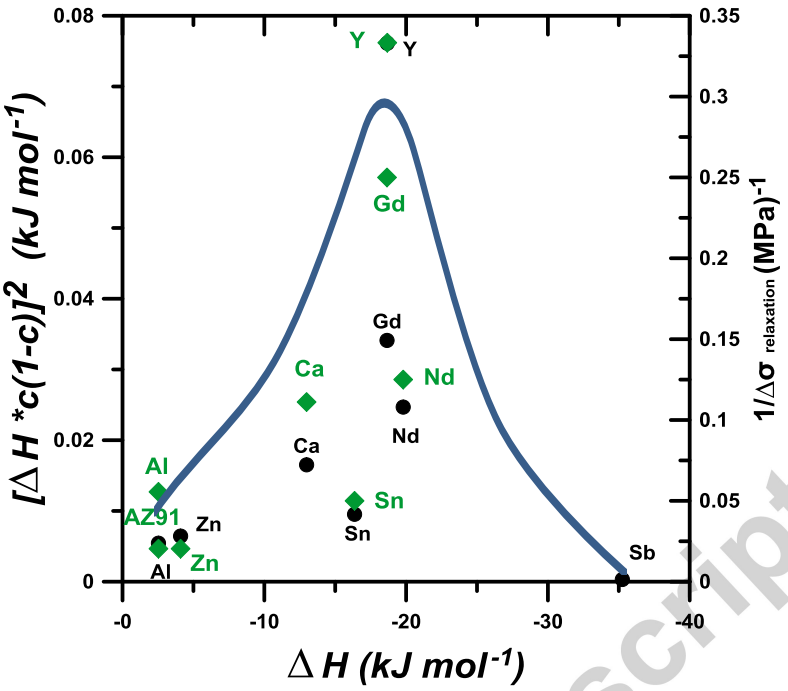

Figure 8. The predicted strength of SRO (circles, left-hand side y-axis) according to Eq.2 (using size corrected values for ΔH, see Appendix A) and stress relaxation data from Fig. 4-a (diamonds, right-hand side y-axis). The line suggests the trend discussed. The respective scales of the left and right hand side y-axes were adjusted for the data to fit within comparable spans.

Conclusions

Ca and Sn introduce a very strong solid solution hardening at room temperature, similar to that of Zn, Y and Gd, and much greater than of Al.

At high temperatures, Ca effectively prevents stress relaxation matching the effect of Y, Gd and Nd, in contrast with Sn and to a lower extent by Zn, which have negligible strengthening effects.

The similar strengthening introduced at room temperature by Ca and Sn in comparison with Zn, Y and the RE is consistent with the presence of SRO, and distinguishes them from Al, which represents a nearly ideal random solid solution.

At high temperature, SRO appears enhanced for atoms larger than Mg, namely: Y, Gd, Nd and Ca. The opposite effect, a relatively weaker than expected SRO, was observed for the solutes smaller than Mg, i.e., Sn and Zn.

Atomic size effects upon the strength of SRO are not very significant at room temperature but they do appear to determine the extent of the athermal regime, making them crucial for the high temperature strength.

References

[1] B.L. Mordike, Materials Science and Engineering A, 324 (2002) 103-112. http://dx.doi.org/10.1016/S0921-5093(01)01290-4.
[2] J.-F. Nie, Metallurgical and Materials Transactions A, 43 (2012) 3891-3939.
[3] A.A. Luo, in: H.I. Kaplan (Ed.) Magnesium Technology, TMS 2002, pp. 42-48
[4] M. Pekguleryuz, M. Celikin, International Materials Reviews, 55 (2010) 197-217. http://dx.doi.org/10.1179/095066010X12646898728327.
[5] Z. Yang, J.P. Li, J.X. Zhang, G.W. Lorimer, J. Robson, Acta Metallurgica Sinica (English Letters), 21 (2008) 313-328.
[6] A. Srinivasan, U.T.S. Pillai, B.C. Pai, Materials Science and Engineering A, 527 (2010) 6543-6550. http://dx.doi.org/10.1016/j.msea.2010.07.020.
[7] M.S. Dargusch, G.L. Dunlop, A.L. Bowles, K. Pettersen, P. Bakke, Metallurgical and Materials Transactions A, 35 (2004) 1905-1909.
[8] A. Srinivasan, J. Swaminathan, M.K. Gunjan, U.T.S. Pillai, B.C. Pai, Materials Science and Engineering A, 527 (2010) 1395-1403. http://dx.doi.org/10.1016/j.msea.2009.10.008.
[9] Y. Guangyin, S. Yangshan, Z. Weiming, Journal of Materials Science Letters, 18 (1999) 2055-2057.
[10] C. Mendis, C. Bettles, M. Gibson, S. Gorsse, C. Hutchinson, Philosophical Magazine Letters, 86 (2006) 443-456.
[11] C.L. Mendis, C.J. Bettles, M.A. Gibson, C.R. Hutchinson, Materials Science & Engineering A, 435 (2006) 163-171.
[12] J.F. Nie, B.C. Muddle, Scripta Materialia, 37 (1997) 1475-1481. http://dx.doi.org/10.1016/S1359-6462(97)00294-7.
[13] A.A. Luo, B.R. Powell, M.P. Balogh, Metallurgical and Materials Transactions A, 33 (2002) 567-574. http://dx.doi.org/10.1007/s11661-002-0118-1.
[14] S. Zhu, M.A. Easton, T.B. Abbott, J.-F. Nie, M.S. Dargusch, N. Hort, M.A. Gibson, Metallurgical and Materials Transactions A, 46 (2015) 1-12. http://dx.doi.org/10.1007/s11661-015-2946-9.
[15] W.E. Mercer II, J.E. Hillis, in, SAE Technical Paper, 1992.http://dx.doi.org/10.4271/920073.
[16] A.A. Luo, M.P. Balogh, B.R. Powell, in, SAE Technical Paper, 2001.http://dx.doi.org/10.4271/2001-01-0423.
[17] S.M. Zhu, M.A. Gibson, M.A. Easton, J.F. Nie, Scripta Materialia, 63 (2010) 698-703.
[18] T. Wang, L. Jiang, R. Mishra, J. Jonas, Metallurgical and Materials Transactions A, 45 (2014) 4698-4709. http://dx.doi.org/10.1007/s11661-014-2371-5.
[19] S. Abaspour, C. Cáceres, Metallurgical and Materials Transactions A, 46 (2015) 5972-5988. http://dx.doi.org/10.1007/s11661-015-3128-5.
[20] R. Tendler, J.P. Abriata, Journal of Nuclear Materials, 150 (1987) 251-258. http://dx.doi.org/10.1016/0022-3115(87)90001-8.
[21] N. Stanford, Materials Science and Engineering A, 528 (2010) 314-322.
[22] D. Griffiths, Materials Science and Technology, 31 (2015) 10-24.
[23] I. Toda-Caraballo, E.I. Galindo-Nava, P.E.J. Rivera-Díaz-del-Castillo, Acta Materialia, 75 (2014) 287-296.
[24] C. Corby, C.H. Cáceres, P. Lukác, Materials Science and Engineering A, 387-389 (2004) 22-24. http://dx.doi.org/doi:10.1016/j.msea.2004.01.077.
[25] S.M. Zhu, M.A. Gibson, J.F. Nie, M.A. Easton, T.B. Abbott, Scripta Materialia, 58 (2008) 477-480. http://dx.doi.org/10.1016/j.scriptamat.2007.10.041.
[26] Z. Trojanova, C.H. Caceres, Scripta Materialia, 56 (2007) 793-796.
[27] C. Wang, Y. Xu, E. Han, Journal of Metallurgy, 2012 (2012) http://dx.doi.org/10.1155/2012/674573.

[28] X.Y. Fang, D.Q. Yi, J.F. Nie, Metallurgical and Materials Transactions A, 40 (2009) 2761-2771.
[29] L. Gao, R.S. Chen, E.H. Han, Journal of Alloys and Compounds, 472 (2009) 234-240.
[30] N. Stanford, D. Atwell, M.R. Barnett, Acta Materialia, 58 (2010) 6773-6783. http://dx.doi.org/10.1016/j.actamat.2010.09.003.
[31] S. Abaspour, C. Cáceres, Metallurgical and Materials Transactions A, 47 (2016) 1313-1321. http://dx.doi.org/10.1007/s11661-015-3292-7.
[32] K. Maruyama, M. Suzuki, S. Hiroyuki, Metallurgical and Materials Transactions A, 33 (2002) 875-882.
[33] M.A. Gibson, X. Fang, C.J. Bettles, C.R. Hutchinson, Scripta Materialia, 63 (2010) 899-902. http://dx.doi.org/10.1016/j.scriptamat.2010.07.002.
[34] D.H. Kim, J.Y. Lee, H.K. Lim, J.S. Kyeong, W.T. Kim, D.H. Kim, Materials Transactions, 49 (2008) 2405-2413.
[35] B.Q. Shi, R.S. Chen, W. Ke, Journal of Alloys and Compounds, 509 (2011) 3357-3362.
[36] C.H. Cáceres, D.M. Rovera, Journal of Light Metals, 1/3 (2001) 151-156.
[37] D.S. Gencheva, A.A. Katsnel'son, L.L. Rokhlin, V.M. Silonov, F.A. Khavadzha, Fiz. metal. metalloved., 51 (1981) 788-793.
[38] J. van der Planken, A. Deruyttere, Acta Metallurgica, 17 (1969) 451-454.
[39] S. Henes, V. Gerold, Zeitschrift fur Metallkunde, 53 (1962) 703-708.
[40] V.M. Silonov, E.V. Evlyukhina, L.L. Rokhlin, Russian Physics Journal, 39 (1996) 622-625.
[41] L.A. Safronova, A.A. Katsnel'son, S.V. Sveshnikov, Y.M. L'Vov, Fiz. metal. metalloved., 43 (1977) 76-80.
[42] A. Boos, S. Steeb, Physics Letters A, 63 (1977) 333-334. http://dx.doi.org/10.1016/0375-9601(77)90921-5.
[43] N. Jha, A.K. Mishra, Journal of Alloys and Compounds, 329 (2001) 224-229.
[44] M. Nishijima, K. Hiraga, Materials Transactions, 48 (2007) 10-15.
[45] A.R. Miedema, F.R. de Boer, R. Boom, Calphad, 1 (1977) 341-359. http://dx.doi.org/10.1016/0364-5916(77)90011-6.
[46] A.R. Miedema, Journal of the Less Common Metals, 32 (1973) 117-136. http://dx.doi.org/10.1016/0022-5088(73)90078-7.
[47] A.R. Miedema, R. Boom, F.R. De Boer, Journal of the Less Common Metals, 41 (1975) 283-298. http://dx.doi.org/10.1016/0022-5088(75)90034-x.
[48] F.R. de Boer, R. Boom, W.C.M. Mattens, A.R. Miedema, A.K. Niessen, North-Holland, Amsterdam, 1989.
[49] K.C. Russell, Kinetic processes in advanced alloys, (1989) http://www.dtic.mil/dtic/tr/fulltext/u2/a212049.pdf.
[50] R.F. Zhang, S.H. Sheng, B.X. Liu, Chemical Physics Letters 442 (2007) 511.
[51] J.H. Zhu, C.T. Liu, L.M. Pike, P.K. Liaw, Intermetallics, 10 (2002) 579-595. http://dx.doi.org/10.1016/S0966-9795(02)00030-4.
[52] X.-Q. Chen, W. Wolf, R. Podloucky, P. Rogl, Intermetallics, 12 (2004) 59-62. http://dx.doi.org/10.1016/j.intermet.2003.07.003.
[53] Y.M. Zhang, J.R.G. Evans, Y. Shoufeng, The Journal of Crystallization Physics and Chemistry, 1 (2010) 103-119.
[54] A.R. Miedema, P.F. de Châtel, F.R. de Boer, Physica B+C, 100 (1980) 1-28. http://dx.doi.org/10.1016/0378-4363(80)90054-6.
[55] A.R. Miedema, F.R. De Boer, R. Boom, Physica B+C, 103 (1981) 67-81. http://dx.doi.org/10.1016/0378-4363(81)91003-2.
[56] A.R. Miedema, Physica B: Condensed Matter, 182 (1992) 1-17. http://dx.doi.org/10.1016/0921-4526(92)90565-A.
[57] R. Boom, F.R. De Boer, A.R. Miedema, Journal of the Less Common Metals, 46 (1976) 271-284. http://dx.doi.org/10.1016/0022-5088(76)90215-0.
[58] R.F. Zhang, B.X. Liu, Applied Physics Letters, 81 (2002) 1219-1221. doi:http://dx.doi.org/10.1063/1.1499510.
[59] L. Pauling, Journal of the American Chemical Society, 69 (1947) 542-553.
[60] D. Nagarajan, C.H. Caceres, J.R. Griffiths, submitted, (2016).
[61] M. Salahshoor, Y. Guo, Materials, 5 (2012) 135.
[62] C.H. Cáceres, A. Blake, physica status solidi, 194 (a) (2002) 147-158.

[63] L. Gao, R.S. Chen, E.H. Han, Journal of Alloys and Compounds, 481 (2009) 379-384. http://dx.doi.org/10.1016/j.jallcom.2009.02.131.
[64] D. Kuhlmann-Wilsdorf, Metallurgical and Materials Transactions, 35A (2004) 369-418.
[65] C.H. Cáceres, P. Lukác, Philosophical Magazine A, 88 (2008) 977-989. http://dx.doi.org/10.1080/14786430801968611.
[66] U.F. Kocks, H. Mecking, Progress in Materials Science, 48 (2003) 171-273.
[67] I. Moreno, T. Nandy, J. Jones, J. Allison, T. Pollock, Scripta Materialia, 45 (2001) 1423-1429.
[68] K. Chen, K. Boyle, Metallurgical and Materials Transactions A, 40 (2009) 2751-2760. http://dx.doi.org/10.1007/s11661-009-9954-6.

Appendix A:

Atomic size effects on the standard values of the Miedema energy of formation

Zhang and Lui [58] use the following expression to include atomic size effects on the standard Miedema ΔH values:

$$\Delta H_{\text{B in A}} = \frac{S(c).V_B^{2/3}}{(n_{WS}^{-1/3})_{av}} \times [P(\Delta\varphi^*)^2 + Q(\Delta n_{WS}^{\frac{1}{3}})^2] \qquad \text{Eq A-1}$$

The prefactor S(c) is obtained from:

$$S(c) = 1 - \frac{c_B^s \left| V_A^{2/3} - V_B^{2/3} \right|}{c_A^s V_A^{2/3} + c_B^s V_B^{2/3}}$$

Where $V_B^{2/3}$ and $V_A^{2/3}$ are the surface area of solute and solvent atoms, respectively. c_B^s and c_A^s are the concentration of the solute and solvent surface area calculated from folowing equations:

$$c_A^s = c_A^s V_A^{2/3} / (c_A^s V_A^{2/3} + c_B^s V_B^{2/3})$$

$$c_B^s = c_B^s V_B^{2/3} / (c_A^s V_A^{2/3} + c_B^s V_B^{2/3})$$

Figure 6 and 7 were produced using above equations.